PAPER

Check for updates

Porphyrin–anthracene covalent organic frameworks for sustainable photosterilization†

Jing-Xuan Guo, [ID] [e] Xue-Mei Gao,[cd] Tian-Yue Gu,[c] Hao-Ze Li,[c] Li-Jian Chen, [ID] [abc] Xu Zhao [ID] *[abc] and Xiu-Ping Yan [ID] *[abcd]

Covalent organic frameworks (COFs) have promising applications in enhanced phototherapy. However, COFs that can sustainably play a role in phototherapy without continuous irradiation are extremely scarce. Herein, we report the fabrication of porphyrin–anthracene multifunctional COFs (Por-DPA) for sustainable photosterilization and bacterial-infected wound healing. A porphyrin photosensitizer, as one of the monomers, was used to provide photothermal and photodynamic activities under irradiation. An anthracene derivative, a good chemical source of singlet oxygen ($^1O_2$), was selected as another monomer to capture $^1O_2$ and release it continuously via cycloreversion in the dark. The prepared Por-DPA COF prevents the self-aggregation quenching of the photosensitizer and thermal damage caused by continuous exposure to external light sources. Besides, Por-DPA exhibits good photothermal conversion performance and efficient $^1O_2$ production capacity through dual pathways of photosensitization and cycloreversion. The developed sustainable photosterilization platform not only has good bactericidal effects on *Escherichia coli* and *Staphylococcus aureus*, but also promotes wound healing without obvious side effects, and is expected to be a novel efficient bactericide.

Introduction

Photosterilization, including photothermal and photodynamic sterilization, has attracted much attention in the fields of sterilization and bacterial infection treatment because of its characteristics of low invasiveness, low toxicity, low side effects and lower propensity to produce drug resistance.[1–3] Photosterilization relies on photosensitizers (PSs) to convert the absorbed light energy into heat or generate reactive oxygen species (ROS), especially singlet oxygen ($^1O_2$), thereby inducing local hyperthermia and oxidative stress imbalance at the site of action so as to kill bacteria.[4–6] So far, great efforts in the field of photosterilization have been made and certain progress has been achieved,[7] but some inherent drawbacks still need to be overcome. The bactericidal effect of photosterilization is strongly dependent on the irradiation time and intensity of the external light source.[8] Continuous exposure to an external light source is required to exert its bactericidal effect, which makes thermal damage to adjacent normal tissues unavoidable.[9,10] In addition, conventional small molecule PSs are easy to agglomerate and quench, the lifetime of the ROS produced is short,[11,12] and conventional photodynamic sterilization methods are limited by the lack of oxygen,[13] which all impede the effectiveness of sterilization. Thus, it is highly valuable and challenging to develop a new type of fractionated phototherapy agent, which can continuously exert the phototherapy effect under irradiation and in the dark.

Chemically generated $^1O_2$ offers the possibility of fractionated phototherapy. Endoperoxides (EPOs) have interesting thermodynamic and photochemical properties and have been acknowledged as the most important chemical sources of $^1O_2$.[14,15] For example, polycyclic aromatic derivatives such as anthracene and naphthalene can capture $^1O_2$ to form corresponding EPOs, and the obtained EPOs can further release $^1O_2$ efficiently through the thermal cycloreversion reactions without side reactions.[16–21] It has also been reported that EPOs can produce $^1O_2$, which leads to cell death through a process similar to apoptosis.[7,22–24] It is worth mentioning that the combination of PSs and $^1O_2$-producing molecules from chemical sources is a more sensible

[a] *State Key Laboratory of Food Science and Resources, Jiangnan University, Wuxi 214122, China. E-mail: zhaoxu2017@jiangnan.edu.cn, xpyan@jiangnan.edu.cn*

[b] *International Joint Laboratory on Food Safety, Jiangnan University, Wuxi 214122, China*

[c] *Institute of Analytical Food Safety, School of Food Science and Technology, Jiangnan University, Wuxi 214122, China*

[d] *Key Laboratory of Synthetic and Biological Colloids, Ministry of Education, School of Chemical and Material Engineering, Jiangnan University, Wuxi, 214122, China*

[e] *Dongjiu Campus, Jiangnan University Yixing Graduate School, China*

† Electronic supplementary information (ESI) available. See DOI: https://doi.org/10.1039/d3tb02017g

way to achieve sustainable phototherapy treatment without continuous irradiation.

Covalent organic frameworks (COFs) are a novel type of crystalline porous polymer material that can be modularly synthesized with a clear structure.[25–27] COFs have unique stability and good biocompatibility, and have shown good application prospects in the biomedical field.[28–30] In particular, the rigid ordered porous structure of COFs is beneficial to the storage and transport of $^1O_2$, and can effectively avoid the self-aggregation quenching of PSs (the monomers forming COFs).[31–33] COFs, therefore, have become star materials with great potential for enhancing photodynamic therapy.[34,35] For example, porphyrin-based COFs with acrylate functional units have been designed and used for reaction-enhancing and bacterial-targeted sterilization and wound healing.[36] However, to our knowledge, the design and construction of COFs that can sustainably play a role in phototherapy without continuous irradiation have not been reported.

Herein, we report the design and preparation of a multifunctional COF-based sustainable photosterilization nanoplatform (Por-DPA) material from PS (5,10,15,20-tetra-(4-aminophenyl)porphyrin, TAPP) and the chemical source of $^1O_2$ (9,10-bis(4-formylphenyl)anthracene, DPA) through the Schiff base reaction. The developed Por-DPA COF shows good photothermal conversion ability and $^1O_2$ production capacity under white light irradiation. Notably, Por-DPA can sustainably release $^1O_2$ through cycloreversion without depending on the oxygen concentration after stopping irradiation. Good photothermal conversion capacity and dual-pathway production of $^1O_2$ ability give Por-DPA excellent photosterilization ability. When the concentration of Por-DPA is only 200 μg mL^{-1} under 100 mW cm^{-2} of white light irradiation, the bactericidal efficiency of *Staphylococcus aureus* (*S. aureus*) and *Escherichia coli* (*E. coli*) is as high as 86.1 ± 10.6% and 100.0 ± 0.0%, respectively. Besides, it also shows good ability to promote wound healing without obvious side effects in the bacterium-infected mice model. The prepared Por-DPA COF has broad application prospects in enhancing phototherapy and reducing thermal damage caused by continuous irradiation.

Scheme 1 The design strategy, synthetic route and application principle of the Por-DPA sustainable photosterilization nanoplatform. (a) The design and synthesis of Por-DPA. (b) Illustration of Por-DPA for sustainable photosterilization and wound healing.

This journal is © The Royal Society of Chemistry 2023

J. Mater. Chem. B, 2023, **11**, 11094–11102 | **11095**

Results and discussion

Design, construction and characterization of Por-DPA

Scheme 1 shows the synthetic route and application principle of Por-DPA for sustainable photosterilization and wound healing. To endow the material with good photothermal and sustained photodynamic properties, the photosensitive unit TAPP and the chemical source of $^1O_2$ DPA were selected as monomers, and the required Por-DPA was constructed by the Schiff base reaction. The highly ordered crystal structure is beneficial to the transport of oxygen and the resulting $^1O_2$,[37–39] so the key factors affecting the formation of the COF, such as the reaction solvent, reaction time and reaction temperature, were optimized in detail (Fig. S1, ESI†). As a result, the Por-DPA COF was obtained from TAPP and DPA in a mixture solution of mesitylene/n-butanol (9/1, v/v, 2.0 mL) with 6 mol L^{-1} aqueous acetic acid (0.2 mL) as the catalyst at 120 °C for 3 d. The as-prepared Por-DPA exhibits good photothermal and photodynamic activities under irradiation due to the existence of the TAPP unit and high crystal structure. Meanwhile, DPA captures $^1O_2$ and transforms it into its endoperoxide form. Notably, the resulting DPA peroxide releases $^1O_2$ through cycloreversion, and is converted to DPA again in the dark. Therefore, the photodynamic process can continue during irradiation and in darkness, which in turn is expected to enable sustainable photosterilization.

The crystal structures of the Por-DPA COF were characterized by powder X-ray diffraction pattern (PXRD) and structural simulation. The PXRD spectrum of the Por-DPA COF exhibits several characteristic peaks at 3.5°, 8.1°, 18.0° and 19.4°, and the main peak is similar to the simulated AA stacking model (unit cell parameters $a = b = 33.7047$ Å, $c = 10.5931$ Å, $\alpha = \beta = \gamma = 90°$) (Fig. 1a, b and Table S1, ESI†). The experimental PXRD model coincides well with the pattern after Pawley refinement (R_p and R_{wp} are 4.04% and 5.73% (Fig. 1c)). These results indicate that the obtained Por-DPA possesses a highly ordered crystalline structure with the AA stacking model.

The Por-DPA COF displays a typical C=N stretching vibration band at 1663 cm^{-1} in the FT-IR spectrum, indicating the successful synthesis of the Por-DPA COF (Fig. 1d). Meanwhile, the significant reduction stretching vibration bands of C=O (1697 cm^{-1}) of DPA and N–H of TAPP (3200–3400 cm^{-1}) also confirms the successful formation of C=N due to the Schiff base reaction (Fig. 1d). The morphology of the Por-DPA COF was characterized by scanning electron microscopy (SEM). The results reveal the block morphology of the Por-DPA COF (Fig. S2, ESI†). The stability of the Por-DPA COF was further evaluated by dispersing Por-DPA in different conventional solvents at 25 °C for 2 days. No obvious change in the PXRD patterns and FT-IR spectra was observed (Fig. S3, ESI†), showing the good chemical stability of the Por-DPA COF.

Photothermal and photodynamic performance of Por-DPA

Photothermal conversion performance of Por-DPA in aqueous solution under white light irradiation was first studied. Por-DPA exhibited exposure time, concentration, and power density-dependent temperature increases (Fig. 2a, b and Fig. S4, S5, ESI†).

Specifically, after 100 mW cm^{-2} white light irradiation for 30 min, different concentrations (100 μg mL^{-1}, 200 μg mL^{-1} and 400 μg mL^{-1}) of Por-DPA showed a rapid and obvious temperature increase ($\Delta T = 13.6 \pm 0.4$ °C, 16.0 ± 0.2 °C, and 17.4 ± 0.1 °C, respectively), while the aqueous solution as the control and TAPP (200 μg mL^{-1}, as Por-DPA 400 μg mL^{-1}) showed only slight changes of 4.2 ± 0.1 and 5.9 ± 0.2 °C (Fig. 2a and Fig. S4, ESI†). The above results confirm that unlike TAPP, Por-DPA has excellent photothermal properties. This is mainly due to the strong π–π interaction between COF layers and the high-density ordered packing of TAPP.

9,10-Anthracenediyl-bis(methylene)dimalonic acid (ABDA) was subsequently selected as the $^1O_2$ indicator to investigate the photodynamic properties under irradiation. ABDA could be oxidized by $^1O_2$ resulting in reduced absorbance,[40–42] so it was employed as an indicator. The significant absorbance decrease of ABDA at 377 nm confirmed that Por-DPA produced remarkable $^1O_2$ under irradiation. In addition, the generation efficiency of $^1O_2$ was obviously dependent on the exposure time, concentration and power density (Fig. 2c–e and Fig. S6, S7, ESI†). After 30 min of exposure to 100 mW cm^{-2} white light, the absorbance of ABDA treated with 200 μg mL^{-1} Por-DPA decreased to ca. 13.9 ± 0.2% of the initial value (Fig. 2d and Fig. S6, ESI†). The absorbance of ABDA in Por-DPA (200 μg mL^{-1}) combined with the 30 min white light irradiation group (150 mW cm^{-2}) or Por-DPA (400 μg mL^{-1}) with 30 min irradiation (100 mW cm^{-2}) was close to zero (Fig. 2c–e and Fig. S7, ESI†), which mean that there is significant $^1O_2$ generation. In contrast, neither ABDA alone nor treated with TAPP (100 μg mL^{-1}, equivalent to 200 μg mL^{-1} of Por-DPA) produced obvious $^1O_2$, as the absorbance of ABDA virtually unchanged throughout the whole process (Fig. 2d and Fig. S6, ESI†). These results clearly prove that the ordered structure of Por-DPA availably improves the hydrophilic poor and easy aggregation of TAPP and enhances its ability to produce $^1O_2$, and also proves that Por-DPA is a promising photodynamic material. In addition, no characteristic peak between 500 and 900 nm derived from TAPP was observed in the absorption spectra of different treatment groups, which confirmed that the as-prepared Por-DPA did not degrade under the above treatments and had good stability (Fig. 2c and Fig. S6, S7, ESI†).

1,3-Diphenylisobenzofuran (DPBF), another commonly used $^1O_2$ indicator,[43,44] was further selected to study the sustainable $^1O_2$ production capacity of Por-DPA in the absence of irradiation. The absorbance of DPBF at 410 nm hardly changes within 24 min after the irradiation stopped (Fig. 2f), which confirmed the stability of DPBF under this condition. In contrast, the absorbance of DPBF mixed with pre-excited Por-DPA decreased to about 75.0 ± 0.3% of the initial value (Fig. 2f and Fig. S8, ESI†), confirming that Por-DPA sustainably released $^1O_2$ in the dark. In summary, the obtained Por-DPA has good photothermal properties and dual-pathway $^1O_2$ production activity, holding great promise for sustained photosterilization.

In vitro photosterilization activity of Por-DPA

E. coli (typical Gram-negative bacteria) and S. aureus (typical Gram-positive bacteria) were employed to evaluate the photosterilization
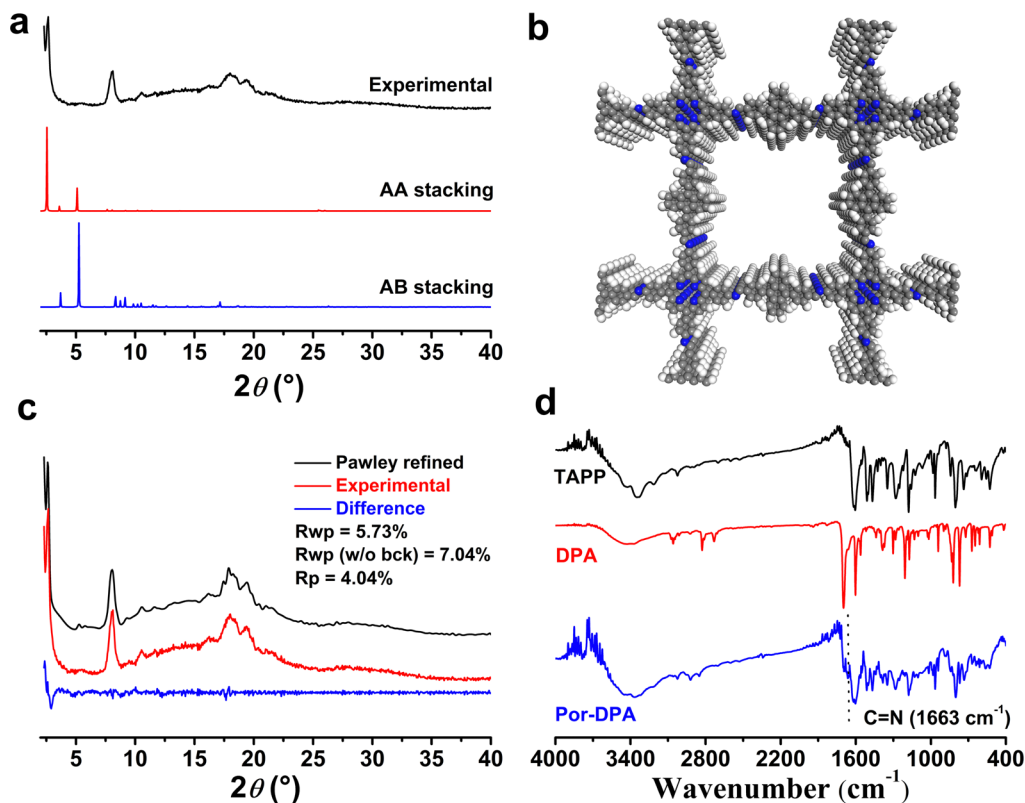
11096 | J. Mater. Chem. B, 2023, 11, 11094–11102

This journal is © The Royal Society of Chemistry 2023

Fig. 1 (a) Simulated (AA and AB stacking models) and experimental PXRD patterns of Por-DPA. (b) Space-filling model of Por-DPA in the AA stacking model (gray C, sky-blue N and white H, respectively). (c) Pawley refinement of Por-DPA. (d) FT-IR spectra of TAPP (black line), DPA (red line) and Por-DPA COF (blue line).
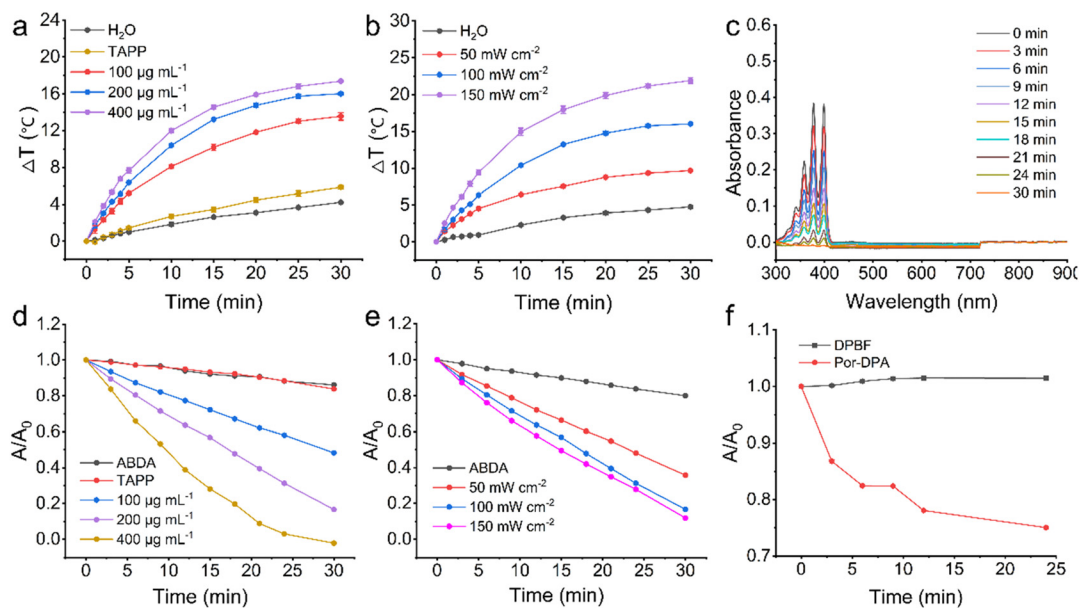

Fig. 2 (a) The time-dependent temperature changes of TAPP (200 μg mL^{-1}) and Por-DPA (100, 200 and 400 μg mL^{-1}, respectively) when irradiated by 100 mW cm^{-2} of white light. (b) Temperature change of Por-DPA (200 μg mL^{-1}) affected by irradiation power. (c) Changes of absorption spectra of ABDA with Por-DPA (400 μg mL^{-1}) under 100 mW cm^{-2} of irradiation. (d) The time-dependent absorbance of ABDA at 377 nm (A/A_0) without and with different concentrations of Por-DPA or TAPP (100 μg mL^{-1}) under irradiation (100 mW cm^{-2}). (e) The time-dependent absorbance (377 nm) of Por-DPA (200 μg mL^{-1}) treated ABDA under different powers of irradiation. A/A_0 is the ratio of the absorbance of ABDA at a certain irradiation time to the initial absorbance of ABDA. (f) Absorbance changes of DPBF at 410 nm with pre-irradiated Por-DPA in the dark (200 μg mL^{-1}).

This journal is © The Royal Society of Chemistry 2023

J. Mater. Chem. B, 2023, **11**, 11094–11102 | **11097**

effect of Por-DPA. The results of the plate colony count showed that Por-DPA presented a significant bactericidal effect under white light irradiation, and the bactericidal effect was positively correlated with the concentration and irradiation time (Fig. 3a, b and Fig. S9, ESI†). The survival rate of *E. coli* co-incubated with 200 μg mL^{-1} Por-DPA was less than 33.8% after 10 min white light irradiation under 100 mW cm^{-2} (Fig. 3a). Exposure to 20 min or more radiation reduced the survival rate of the bacteria to almost zero (Fig. 3a). When treating *E. coli* with higher concentrations of Por-DPA (400 μg mL^{-1}), only 10 min of above irradiation was needed to achieve nearly 100% antibacterial effect (Fig. 3b). In contrast, no obvious change in bacterial viability was observed in *E. coli* treated with white light alone for up to 30 min, indicating that 30 min white light irradiation with this power was relatively safe (Fig. 3a and b). Besides, the survival rate of only Por-DAP treated *E. coli* (200 μg mL^{-1} and 400 μg mL^{-1}) was greater than 90%. While the survival rate of pre-irradiated Por-DAP treated *E. coli* (200 μg mL^{-1} and 400 μg mL^{-1}) was also reduced by $33.9 \pm 5.0\%$ and $39.6 \pm 4.1\%$, respectively (Fig. 3a and b), which could be attributed to the release of $^1O_2$ *via* cycloreversion of Por-DAP in the form of endoperoxide after pre-irradiation. A similar

bactericidal effect against *S. aureus* was also observed (Fig. S9 and S10, ESI†).

The sustainable photosterilization performance of Por-DPA was further confirmed by SEM. The SEM image results showed that the smooth bacterial surface was wrinkled or even cracked after treatment with Por-DPA, especially after Por-DPA combined with irradiation treatment (Fig. 3c). With the extension of irradiation time, the degree of bacterial surface damage was aggravated, and even bacterial membrane rupture and content leakage occur. Contrastingly, the morphology of bacteria treated only by light irradiation was intact, and no significant difference was observed compared with the untreated group (Fig. 3c). These results further confirm that Por-DPA has an excellent photosterilization effect and that the power density of white light used in the experiment is acceptable.

The ROS indicator was further selected to verify the performance of ROS production and sustainable release of $^1O_2$ of Por-DPA. 2,7-Dichlorodihydrofluorescein diacetate, a ROS indicator, can be enzymatically hydrolyzed into cells and oxidized by cytoplasmic ROS to 2′,7′-dichlorofluorescein, which emits strong green fluorescence.[45,46] Under Por-DPA and irradiation
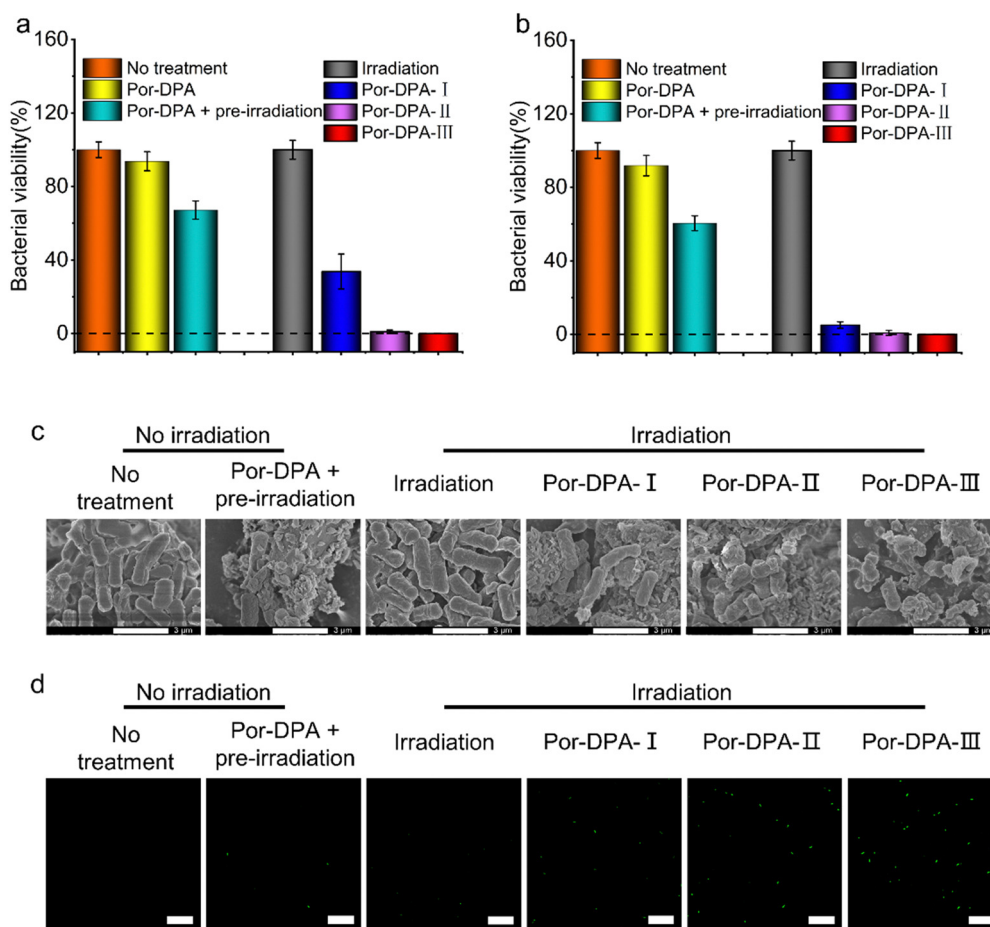

Fig. 3 *In vitro* bacterial viability of *E. coli* incubated with Por-DPA at (a) 200 μg mL^{-1} and (b) 400 μg mL^{-1}, respectively, under different treatments. (c) SEM images of bacteria treated with different ways (scale bar, 3 μm). (d) CLSM images of bacteria treated with different ways for the detection of ROS with green fluorescence (scale bar, 30 μm). Por-DPA-I, Por-DPA-II and Por-DPA-III respectively represented 10, 20 and 30 min irradiation.

11098 | *J. Mater. Chem. B*, 2023, **11**, 11094–11102

This journal is © The Royal Society of Chemistry 2023

treatments, the strong green fluorescence signal of bacteria was observed, and showed irradiation time-dependence (Fig. 3d). Besides, the bacteria treated with pre-irradiation Por-DPA also showed weak green fluorescence. However, neither the untreated bacteria nor the light-treated bacteria showed faint green fluorescence (Fig. 3d). All the above results further indicate that Por-COF has photosensitive and cycloreversion dual-pathways to produce $^1O_2$.

In vivo photosterilization effect of Por-DPA

Encouraged by the excellent *in vitro* sustainable photosterilization performance of Por-DPA, it was further applied to the treatment of bacterial-infected wounds in mice. Firstly, the good biocompatibility of the prepared Por-DPA was proved by the hemolytic assay and MTT test. Even when the concentration of Por-DPA reached 500 µg mL^{-1}, the cell survival rate was still greater than 80%, and the hemolysis rate of red blood cells was still lower than 1% (Fig. S12 and S13, ESI†). Subsequently, the abilities of Por-DPA to treat wound infection and promote wound healing *in vivo* were investigated with the *E. coli*-infected mice model. Infection mice were randomly divided into five groups (n = 5) with different treatments: no treatment, treated with Por-DPA, white light irradiation only, pre-irradiated Por-DPA treatment and Por-DPA combined with irradiation treatment.

As shown in Fig. 4a, the wound area of mice gradually shrank with the extension of treatment time, and obvious inflection points appeared on days 8 to 10. Notably, the wound healing rate of mice treated by Por-DPA combined irradiation was the best among all experimental groups, and the wound area almost disappeared after 12 days of treatment (Fig. 4a and b). In addition, the wound healing speed of pre-irradiated Por-DPA treated mice was slightly faster than that of other control mice (Fig. 4b). The reason is that, on the one hand, Por-DPA can accelerate wound healing through photothermal/photodynamic synergistic effects in the existence of white light irradiation. On the other hand, Por-DPA can continuously release $^1O_2$ through the cycloreversion of endoperoxide formed during the production of $^1O_2$ by irradiation. Meanwhile, no significant fluctuations in the
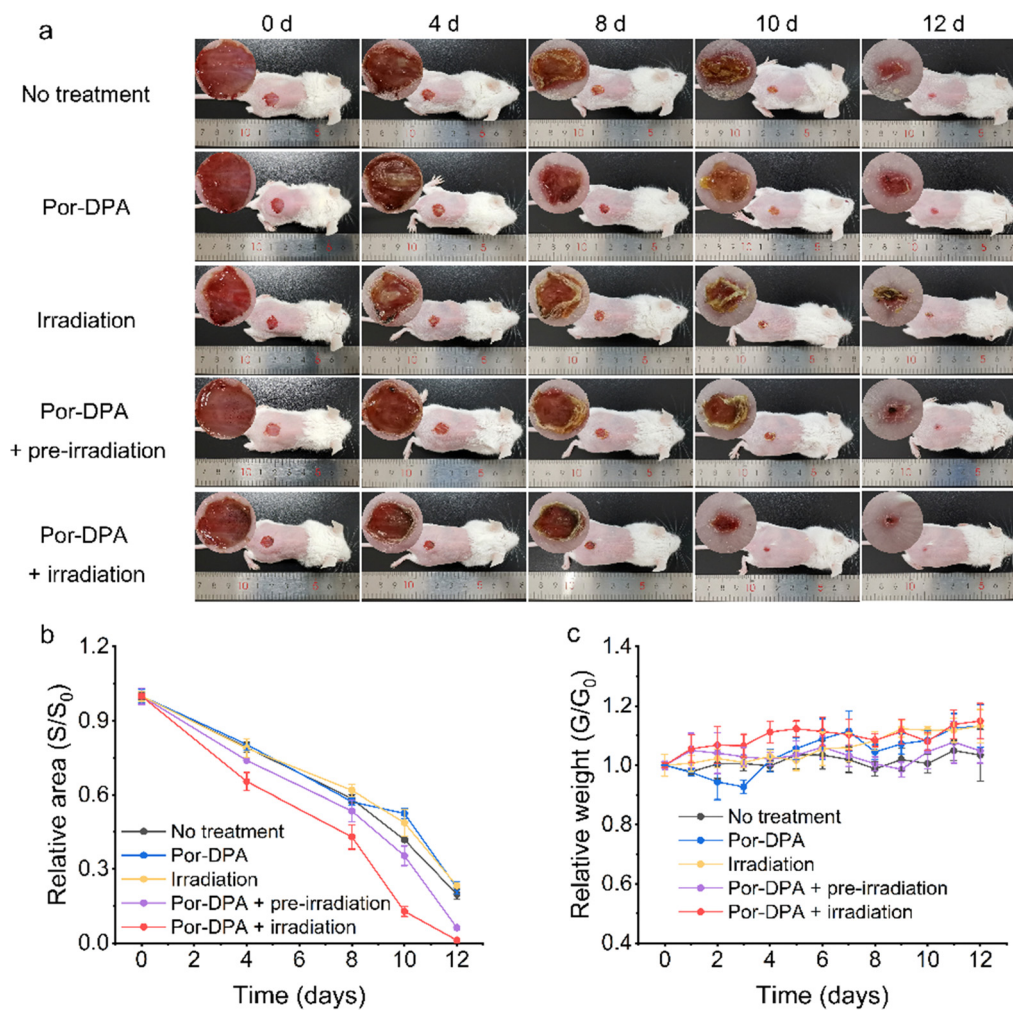

Fig. 4 (a) Representative photographs from different groups of mice. (b) The relative wound areas on days 0, 4, 8, 10 and 12. S/S_0 is the wound area ratio of a certain therapy point to before treatment. (c) Relative body weights of different groups of mice during the whole treatment process. G/G_0 is the ratio of the weight at a certain therapy point to the initial weight.
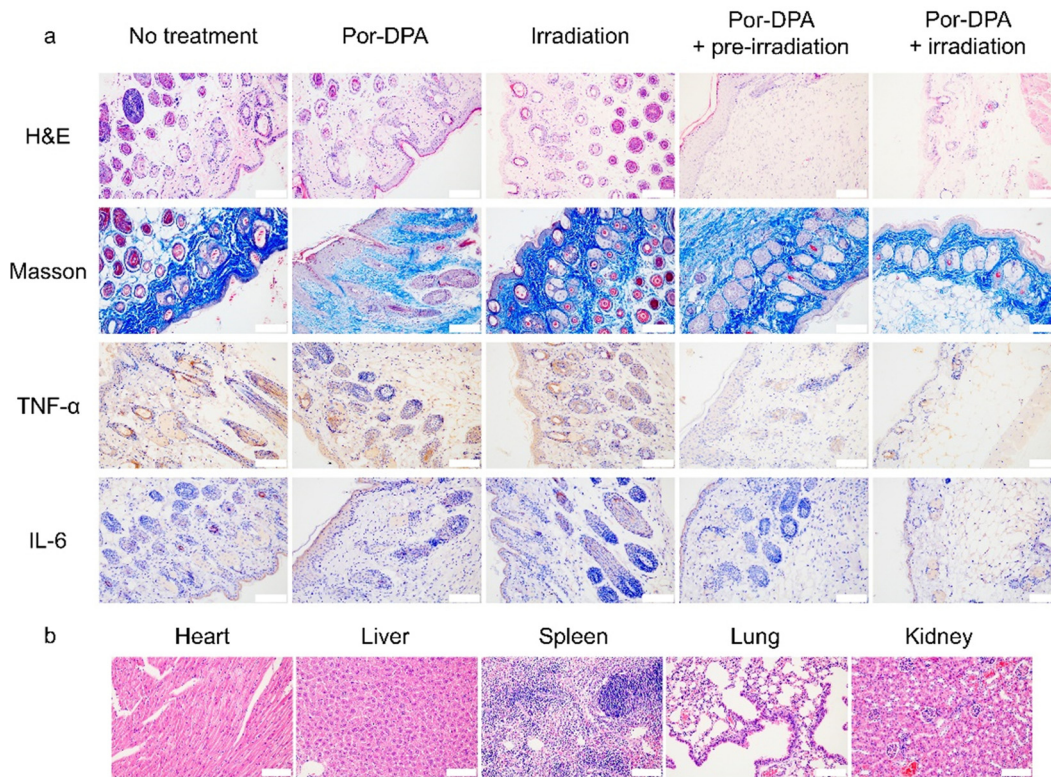
This journal is © The Royal Society of Chemistry 2023

J. Mater. Chem. B, 2023, **11**, 11094–11102 | **11099**

Fig. 5 (a) The wound staining of mice after 12 day different treatments (scale bars of H&E, Masson, TNF-α, and IL-6 are 200 μm; 200 μm, 100 μm, and 100 μm, respectively). (b) H&E staining of the main organs of Por-DPA-treated mice under irradiation (scale bar, 200 μm).

weight of mice were observed, showing that all mice were in a healthy state during the treatment (Fig. 4c).

H&E staining and Masson staining of wounds were performed to further evaluate the therapy efficacy of Por-DPA. The Por-DPA combined with the white light irradiation group or the pre-irradiated Por-DPA treatment group showed a large amount of collagen tissue and very few inflammatory cells (Fig. 5a). In contrast, a large number of inflammatory cells and a small amount of collagen tissue appeared in the control group (Fig. 5a). In addition, the pre-irradiated Por-DPA-treated group and the Por-DPA combined white light irradiation group had much less TNF-α and IL-6 than the other groups (Fig. 5a). These results again show that Por-DPA can effectively kill bacteria and promote wound healing through photothermal/ photodynamic effects under irradiation, while Por-DPA can further improve sterilization and promote wound healing by spontaneously releasing $^1O_2$ in the dark. Furthermore, H&E staining results of major organs in mice showed no significant side effects of these treatments (Fig. 5b and Fig. S14, ESI†). In summary, Por-DPA has excellent photosterilization properties and has good application prospects in accelerating infected-wound healing and skin regeneration.

Conclusions

In summary, we have selected the photosensitizer TAPP and the chemical source $^1O_2$ DPA as monomers, and synthesized a multifunctional COF (Por-DPA) by a hydrothermal method for sustainable photosterilization and infected-wound healing. The highly ordered crystal structure of the COF prevents the self-aggregation quenching of TAPP and facilitates the storage and transfer of $^1O_2$. Por-DPA has good photothermal conversion performance and $^1O_2$ production ability under irradiation. Importantly, Por-DPA can continue to release $^1O_2$ through spontaneous conversion of DPA endoperoxide produced upon irradiation to DPA. Excellent photothermal properties combined with efficient $^1O_2$ production capacity by photosensitization and cycloreversion pathways endow the prepared Por-DPA with efficient bactericidal effects and accelerated wound healing. Moreover, the prepared Por-DPA has good stability, excellent cytocompatibility and negligible systemic toxicity, showing good application prospects.

Author contributions

Jing-Xuan Guo: conceptualization, investigation, validation, methodology, data curation, formal analysis, and writing – original draft. Xue-Mei Gao and Tian-Yue Gu: investigation, data curation, and formal analysis. Hao-Ze Li: data analysis. Li-Jian Chen: validation and supervision. Xu Zhao: conceptualization, methodology, validation, supervision, funding acquisition, and writing – review and editing. Xiu-Ping Yan: supervision, funding acquisition, and writing – review and editing. All authors have read and approved the final submitted manuscript.

11100 | J. Mater. Chem. B, 2023, **11**, 11094–11102

This journal is © The Royal Society of Chemistry 2023

Conflicts of interest

There are no conflicts to declare.

Acknowledgements

Notes and references

1 B. Wang, L. Zhou, Y. Guo, H. Guo, Y. Zhong, X. Huang, Y. Ge, Q. Wang, X. Chu, Y. Jin, K. Lan, M. Yang and J. Qu, *Bioact. Mater.*, 2022, **12**, 314–326.

2 A. Kamkaew, S. H. Lim, H. B. Lee, L. V. Kiew, L. Y. Chung and K. Burgess, *Chem. Soc. Rev.*, 2013, **42**, 77–88.

3 S. Yougbare, C. Mutalik, P. F. Chung, D. I. Krisnawati, F. Rinawati, H. Irawan, H. Kristanto and T. R. Kuo, *Nanomaterials*, 2021, **11**, 3064.

4 K. Han, Z. Ma and H. Han, *J. Mater. Chem. B*, 2018, **6**, 25–38.

5 S. Song, G. Xu, N. Yang, S. A. Shahzad, J. Lv, X. Shen and C. Yu, *J. Mater. Sci.*, 2022, **57**, 21206–21218.

6 J. Zhu, J. Zou, J. Zhang, Y. Sun, X. Dong and Q. Zhang, *J. Mater. Chem. B*, 2019, **7**, 3303–3309.

7 G. Li, M. Wu, Y. Xu, Q. Wang, J. Liu, X. Zhou, H. Ji, Q. Tang, X. Gu, S. Liu, Y. Qin, L. Wu and Q. Zhao, *Coord. Chem. Rev.*, 2023, **478**, 214979.

8 M. Lan, S. Zhao, Z. Zhang, L. Yan, L. Guo, G. Niu, J. Zhang, J. Zhao, H. Zhang, P. Wang, G. Zhu, C.-S. Lee and W. Zhang, *Nano Res.*, 2017, **10**, 3113–3123.

9 Y. Jiang, Z. Tan, T. Zhao, J. Wu, Y. Li, Y. Jia and Z. Peng, *Nanoscale*, 2023, **15**, 1925–1936.

10 X. Li, W. Bao, M. Liu, J. Meng, Z. Wang, M. Sun, L. Zhang and Z. Tian, *Biomater. Sci.*, 2022, **10**, 5520–5534.

11 L. Wang, L. Tang, Y. Liu, H. Wu, Z. Liu, J. Li, Y. Pan and E. U. Akkaya, *Chem. Commun.*, 2022, **58**, 1902–1905.

12 X. Li, S. Lee and J. Yoon, *Chem. Soc. Rev.*, 2018, **47**, 1174–1188.

13 Y. Zhang, F. Wang, C. Liu, Z. Wang, L. Kang, Y. Huang, K. Dong, J. Ren and X. Qu, *ACS Nano*, 2018, **12**, 651–661.

14 Y. Zhao, M. Sun, X. Wang, C. Wang, D. Lu, W. Ma, S. A. Kube, J. Ma and M. Elimelech, *Nat. Commun.*, 2020, **11**, 6228.

15 Y. Ni, W. Fang, K. K. Baldridge and M. A. Olson, *Chem. – Eur. J.*, 2023, **29**, e202300624.

16 Y. Zhu, Y. Yang, N. Li, C. Luo and X. Hou, *Chem. Eng. J.*, 2022, **446**, 137333.

17 J. Shen, L. Pan, X. Zhang, Z. Zou, B. Wei, Y. Chen, X. Tang and D. Zou, *Front. Bioeng. Biotechnol.*, 2022, **10**, 781766.

18 Z. Yuan, S. Yu, F. Cao, Z. Mao, C. Gao and J. Ling, *Polym. Chem.*, 2018, **9**, 2124–2133.

19 M. Kucukoflaz, S. Ulusoy, B. Korkmaz, S. C. Ozturk, M. Akyol, S. B. Hayta, O. F. Goze, G. Esendagli and F. Sozmen, *J. Nanopart. Res.*, 2023, **25**, 62.

20 T. Homma, S. Kobayashi and J. Fujii, *Biochem. Biophys. Res. Commun.*, 2019, **518**, 519–525.

21 M. A. Filatov and M. O. Senge, *Mol. Syst. Des. Eng.*, 2016, **1**, 258–272.

22 Z. Yuan, S. Yu, F. Cao, Z. Mao, C. Gao and J. Ling, *Polym. Chem.*, 2018, **9**, 2124–2133.

23 H. Hu, X. Yan, H. Wang, J. Tanaka, M. Wang, W. You and Z. Li, *J. Mater. Chem. B*, 2019, **7**, 1116–1123.

24 W. Xiao, P. Wang, C. Ou, X. Huang, Y. Tang, M. Wu, W. Si, J. Shao, W. Huang and X. Dong, *Biomaterials*, 2018, **183**, 1–9.

25 K. Geng, T. He, R. Liu, S. Dalapati, K. T. Tan, Z. Li, S. Tao, Y. Gong, Q. Jiang and D. Jiang, *Chem. Rev.*, 2020, **120**, 8814–8933.

26 Y. Cheng, L. Zhai, Y. Ying, Y. Wang, G. Liu, J. Dong, D. Z. L. Ng, S. A. Khan and D. Zhao, *J. Mater. Chem. A*, 2019, **7**, 4549–4560.

27 J. Li, X. Jing, Q. Li, S. Li, X. Gao, X. Feng and B. Wang, *Chem. Soc. Rev.*, 2020, **49**, 3565–3604.

28 X. Guan, Q. Fang, Y. Yan and S. Qiu, *Acc. Chem. Res.*, 2022, **55**, 1912–1927.

29 Z. Wang, S. Zhang, Y. Chen, Z. Zhang and S. Ma, *Chem. Soc. Rev.*, 2020, **49**, 708–735.

30 R. K. Sharma, P. Yadav, M. Yadav, R. Gupta, P. Rana, A. Srivastava, R. Zbořil, R. S. Varma, M. Antonietti and M. B. Gawande, *Mater. Horiz.*, 2020, **7**, 411–454.

31 L. A. Baldwin, J. W. Crowe, D. A. Pyles and P. L. McGrier, *J. Am. Chem. Soc.*, 2016, **138**, 15134–15137.

32 R. Liu, K. T. Tan, Y. Gong, Y. Chen, Z. Li, S. Xie, T. He, Z. Lu, H. Yang and D. Jiang, *Chem. Soc. Rev.*, 2021, **50**, 120–242.

33 J. Y. Zeng, X. S. Wang, Y. D. Qi, Y. Yu, X. Zeng and X. Z. Zhang, *Angew. Chem., Int. Ed.*, 2019, **58**, 5692–5696.

34 J. Zou, J. Zhu, Z. Yang, L. Li, W. Fan, L. He, W. Tang, L. Deng, J. Mu, Y. Ma, Y. Cheng, W. Huang, X. Dong and X. Chen, *Angew. Chem., Int. Ed.*, 2020, **59**, 8833–8838.

35 M. H. Zhang, J. Fang, Y. Z. Liu, Y. J. Wang, L. Liao, L. X. Tang, L. K. Zhu, S. L. Qiu and Q. R. Fang, *Small Struct.*, 2021, **2**, 2000108.

36 G. Lin, H. Ding, R. Chen, Z. Peng, B. Wang and C. Wang, *J. Am. Chem. Soc.*, 2017, **139**, 8705–8709.

37 C. Xing, Y. Zhang, D. Wei, C. Zhang and L. Zhao, *New J. Chem.*, 2023, **47**, 5160–5163.

38 Y. Huang, X. Hao, S. Ma, R. Wang and Y. Wang, *Chemosphere*, 2022, **291**, 132795.

39 E. Dautzenberg, M. Lam, T. Nikolaeva, W. M. J. Franssen, B. van Lagen, I. P. A. M. Gerrits-Benneheij, N. Kosinov, G. Li and L. C. P. M. de Smet, *J. Phys. Chem. C*, 2022, **126**, 21338–21347.

40 M.-C. Wang, J.-X. Guo, L.-J. Chen and X. Zhao, *Biomater. Sci.*, 2023, **11**, 1776–1784.

41 D.-H. Wang, L.-J. Chen, X. Zhao and X.-P. Yan, *J. Mater. Chem. B*, 2021, **9**, 9900–9907.

42 H. Zhang and X.-B. Yin, *ACS Appl. Mater. Interfaces*, 2022, **14**, 26528–26535.

This journal is © The Royal Society of Chemistry 2023

J. Mater. Chem. B, 2023, **11**, 11094–11102 | 11101

43 J. Zou, J. Zhu, Z. Yang, L. Li, W. Fan, L. He, W. Tang, L. Deng, J. Mu, Y. Ma, Y. Cheng, W. Huang, X. Dong and X. Chen, *Angew. Chem., Int. Ed.*, 2020, **59**, 8833–8838.

44 J. Zou, L. Li, J. Zhu, X. Li, Z. Yang, W. Huang and X. Chen, *Adv. Mater.*, 2021, **33**, e2103627.

45 B. Tian, S. Liu, C. Yu, S. Liu, S. Dong, L. Feng, N. Hu and P. Yang, *Adv. Funct. Mater.*, 2023, **33**, 2300818.

46 Y. Zhu, M. Gao, M. Su, Y. Shen, K. Zhang, B. Yu and F. J. Xu, *Angew. Chem., Int. Ed.*, 2023, **62**, e202306803.